Efimov-Like Behaviour in Low-Dimensional Polymer Models

Federica Mura[1] · Somendra M. Bhattacharjee[2] ·
Jaya Maji[3] · Mario Masetto[4] · Flavio Seno[4,5] ·
Antonio Trovato[4,6]

Abstract In the quantum Efimov effect, identical bosons form infinitely many bound trimer states at the bound dimer dissociation threshold, with their energy spectrum obeying a universal geometrical scaling law. Inspired by the formal correspondence between the possible trajectories of a quantum particle and the possible conformations of a polymer chain, the existence of a triple-stranded DNA bound state when a double-stranded DNA is not stable was recently predicted by modelling three directed polymer chains in low-dimensional lattices, both fractal ($d < 1$) and euclidean ($d = 1$). A finite melting temperature for double-stranded DNA requires in $d \leq 2$ the introduction of a weighting factor penalizing the formation of denaturation bubbles, that is non-base paired portions of DNA. The details of how bubble weighting is defined for a three-chain system were shown to crucially affect the presence of Efimov-like behaviour on a fractal lattice. Here we assess the same dependence on the euclidean $1 + 1$ lattice, by setting up the transfer matrix method for three infinitely long chains confined in a finite size geometry. This allows us to discriminate unambiguously between the absence of Efimov-like behaviour and its presence in a very narrow temperature range, in close

✉ Antonio Trovato
antonio.trovato@unipd.it

[1] Department of Physics, Ludwig-Maximilians-Universität München, Theresienstrasse 37, 80333 Munich, Germany

[2] Institute of Physics, Bhubaneswar 751 005, India

[3] Institute of Mathematical Sciences, Chennai 600 113, India

[4] Physics and Astronomy Department "G. Galilei", Padova University, via Marzolo 8, 35131 Padua, Italy

[5] National Institute for Nuclear Physics (INFN), Padova Section, via Marzolo 8, 35131 Padua, Italy

[6] National Interuniversity Consortium for the Physical Sciences of Matter (CNISM), Padova Unit, via Marzolo 8, 35131 Padua, Italy

correspondence with what was already found on the fractal lattice. When present, however, no evidence is found for triple-stranded bound states other than the ground state at the two-chain melting temperature.

Keywords Efimov effect · Triplex DNA · Poland–Scheraga model · Transfer matrix

1 Introduction

The Efimov effect was first predicted by Efimov in 1970 [1] for identical bosons that occupy a spatially symmetric s-state and interact with a short-range pair-wise potential. When the two-body state is exactly at the dissociation threshold, the trimer spectrum obeys a geometrical scaling law, such that the ratio of the successive energy eigenvalues of the system is a constant and accumulation of states near zero energy takes place [2]. Infinitely many three-body bound states are stable when two-body ones are not. Efimov physics is universal and does not depend on the details of the pair-wise potential, which could occur, for example, between atoms with a van der Waals interaction, or between halo nuclei with a nuclear force [3]. Efimov trimers are loose states with sizes much larger than the short range of the pair-wise interaction. In the last decade, Efimov states were experimentally detected and characterized in the context of quantum gases with ultracold atoms [4].

In recent years, the analogue of Efimov behaviour in the context of polymer physics was suggested [5–9], relying on the well-known formal correspondence between free particle trajectories in quantum mechanics and continuous flexible Gaussian polymer chains, whereby the imaginary time along the quantum trajectory is equivalent to the polymer contour length. The partition function of a Gaussian chain with elastic constant κ and total contour length s at temperature T, expressed as a path integral over all possible trajectories $\mathbf{r}\left(s'\right)$: $Z = \int \mathcal{DR} \exp\left[-\beta \int_0^s \mathrm{d}s' \frac{\kappa}{2} \left(\frac{\partial \mathbf{r}}{\partial s'}\right)^2\right]$, is formally equivalent to the Green's function at time t of a free quantum particle with mass m by using $\frac{\hbar}{m} = \frac{1}{\beta\kappa} = \frac{K_B T}{\kappa}$; $s = it$. The infinite time limit, with the ensuing ground state dominance, corresponds to the thermodynamic limit $s \to \infty$ of an infinitely long polymer. As two particles interacting with each other do so only at the same time, the corresponding polymeric constraint yields, for a discrete chain, the sequential base pairing typical of the Poland–Scheraga DNA-like polymer model: only monomers with the same chain index interact with each other [10]. A quantum two-body bound state, stabilized by the interaction potential, corresponds to a double-stranded DNA, stabilized through Watson–Crick base pairing. Quantum fluctuations in the classically forbidden regions corresponds to thermal fluctuations opening portions within double-stranded DNA, called bubbles. The overall melting of double- stranded DNA, achieved by raising the temperature, is equivalent to the disappearance of a stable bound state obtained by decreasing the strength of the two-body potential. In close analogy with the related quantum problem, the above happens in $d = 3$; in low dimension $d \leq 2$, a bound state always exists for an arbitrarily weak short-range attractive potential, and a double-stranded DNA is correspondingly stable at any finite temperature.

The Efimov state is naturally translated within the polymer DNA-like context as a triple-stranded DNA state that is stable when a double-stranded DNA is not. It is

indeed well known that a double-stranded DNA allows a third strand to bind via the Hoogsteen or the reverse Hoogsteen pairing to form a triple helix [11,12]. NMR experiments show that Hoogsteen pairing can be formed dynamically (1 % of time) even in a normal DNA [13]. The formation of a triple helix controls the gene expression, with possible therapeutic applications such as developing antibiotics [14] and targeting a specific sequence in gene therapy [15]. The short range of both Watson–Crick and Hoogsteen pairings is determined by the hydrogen bond length. The hypothesized Efimov-DNA, however, would be a loosely bound state that should not depend on a specific pairing mechanism and be stable only close to the double-stranded DNA melting temperature.

We already addressed the study of the Efimov effect in polymer physics by employing low-dimensional lattice models. We could then perform exact analytical computations in the thermodynamic limit on fractal lattices [8] and carry on exact finite size enumerations on euclidean lattices [5]. In the latter case, which is also the focus of the present study, discrete polymer chains are considered, whereas the quantum mapping holds rigorously for continuous polymer chains. One price to pay in low dimensions ($d \leq 2$) is that the formation of DNA bubbles needs to be penalized by either a non-crossing constraint [16] or an "ad-hoc" weight in order for the melting temperature of the two-chain problem to be finite. Bubble weighting is indeed extensively used to take into account the cooperativity of stacking interactions between consecutive base pairs in realistic DNA modelling [17], yet its mapping onto the quantum formalism would require additional care.[1] At the same time, bubble weighting can be introduced in different ways when dealing with the opening/closing of a three-stranded DNA portion, so that several models can be devised [5,8]. As a result, we were able to demonstrate the presence of an Efimov-like feature, that is the stability of a triple-stranded DNA in a narrow temperature range *above* the double-stranded melting temperature, but only within some of the considered models. On top of that, the presence of the Efimov signature could depend on the kind of lattice used, either fractal or euclidean.

A yet unanswered question concerns the possibility of finding the full spectrum of Efimov triplet DNA states, verifying the universal geometrical scaling law. It should be noted, in this respect, that the quantum Efimov effect for identical bosons only occurs for a narrow range of dimensions, $2.30 < d < 3.76$ [18]. On the other hand, bubble weighting, chain discreteness, and the absence of quantum statistics may alter the Efimov properties that are known from quantum mechanics, leading to a possibly different, yet related, three-body polymer physics.

Here, we address the role of three-chain bubble weighting within a low-dimensional euclidean lattice model. More specifically, we model DNA chains with N steps (bases) that can cross each other using the Poland–Scheraga recipe for directed self-avoiding polymers in a $1 + 1$ square lattice. Bubble formation between strand pairs is weighted by a fugacity σ (see Sect. 2). We consider a two-body Boltzmann weight $y = \exp(-\beta\epsilon)$ for all possible base pairs. A base triplet is given the two-body contribution due to

---

[1] The mapping of bubble weighting onto the quantum formalism might be possible by introducing a tunnelling coefficient through a δ-potential barrier at the boundary of a short-range square well. Hermiticity would, however, require both the opening and the closing of bubbles to be given the same weight.

all three base pairs within it, together with a pure three-body Boltzmann weight $w = \exp(-\beta\eta)$, yielding an overall weight $y^3 w = \exp(-3\epsilon - \eta)$. Throughout all this work, we choose $w = 1/y$, so that $y^3 w = y^2 = \exp(-2\epsilon)$ and the three-chain melting transition temperature is the same as the two-chain one if a Y-fork model where bubble formation is suppressed ($\sigma = 0$) is considered [5]. On the other hand, the possibility of forming bubbles is crucial for the Efimov-like effect [5], and we use $\sigma = 1/2$ in order to have a finite melting transition temperature $y_{2,t} = 4/3$ (see Sect. 2). The opening (closing) of a three-chain bubble can happen in our model only by separating (joining) a double- and a single-stranded portion (see Fig. 1). Three-chain bubble formation is then given the two-body contribution due to the two different two-chain bubbles that form, together with a pure three-chain bubble fugacity ρ, yielding an overall weight $\sigma^2 \rho$.

It is important to observe that, both within the classic Poland–Scheraga approach [19], further revisited to study DNA overstretching by a pulling force [20], and within more refined models for real DNA molecules [17], the entropic weight $f(l)$ due to bubbles of size l is modelled explicitly $f(l) \sim l^{-c}$ through the knowledge of the so-called reunion exponent c.[2] On the other hand, within our model, the entropic contribution of bubbles to the partition function is already taken care of exactly by the enumeration of all possible conformations. Bubble fugacity parameters can thus be seen as extra-weights, which are in principle related to the cooperativity of stacking interactions between consecutive base pairs or base triplets [17]. The energy parameters ϵ and η in our model are in principle related to base pairs dissociation free energies in more realistic models that take into account both nucleotide and solvent degrees of freedom [17].

Our aim is to verify whether the three-chain melting transition temperature is higher than the two-chain one ($y_{3,t} < y_{2,t}$), evidencing a temperature window for $y_{3,t} < y < y_{2,t}$ where a double-stranded state is not stable, whereas a triple-stranded state is stable, akin to the Efimov effect in quantum mechanics.

We had previously claimed that such an effect is present in the directed $1+1$ square lattice model where three-chain bubble formation is weighted by an overall σ^2 factor, obtained by choosing $\rho = 1$ [5]. We called this Model A. That conclusion was based on the extrapolation of finite size transition temperature estimates obtained by evaluating the partition function of a three-chain unconfined system within an iterative transfer matrix approach (see Sect. 2). Finite size estimates were obtained by evaluating the temperatures where rescaled end-to-end distance curves for different sizes cross each other up to a size (chain length) of $N \simeq 4000$. In particular, bubble fugacity was implemented in [5] by weighting both bubble closing and opening. A different possibility, employed in this work, is to weight either only closing, or only opening. Different realizations provide different finite size estimates, but all should yield the same result in the thermodynamic limit $N \to \infty$.

---

[2] The value of the reunion exponent c is related to the order of the melting transition of double-stranded DNA and was computed for a fully self-avoiding (i.e. non-directed) $d = 3$ polymer model [19]. The values of the reunion exponent for several directed polymers are known exactly in $d = 1$ [21] and through renormalization group estimates in generic dimension [22].

Subsequently, however, we found that a similar model ($w = 1/y$ and σ^2 factor associated to three-chain bubble formation, called $TS2$ model in that context) did not show a similar Efimov-like effect, when defined on a fractal Sierpinski gasket, for which $d + 1 = \ln 3 / \ln 2 < 2$. A different model (called $TS3$ in that context) was instead found to exhibit the Efimov-like effect $y_{3,t} < y_{2,t}$ on the Sierpinski gasket. In this model, that we call Model C here, $w = 1/y$ and three-chain bubble formation is weighted by an overall σ factor, obtained by choosing $\rho = 1/\sigma$. The fractal lattice results were based on an exact renormalization group computation [8].

This conflicting result could be ascribed to the different nature (euclidean vs. fractal) of the used lattices. Yet, it appears particularly paradoxical since three-chain bubble formation is less favoured in Model A than in Model C, implying that the triple-stranded state is expected to be more stable in model C, because of the entropy gain due to enhanced bubble formation. The Efimov-like behaviour found on the fractal lattice would seem thus sensible in this respect.

Here, we reconsider Model A and we compare it to Model C for directed chains in a $1 + 1$ square lattice. In order to achieve a better extrapolation in the thermodynamic limit, we undertake two different strategies, both fully exploiting the symmetries of the system (see Sect. 2 and Fig. 1). On the one hand, we compute finite size estimates of the three-chain melting temperature for the unconfined system as we already did [5]. We consider two alternative realizations for weighting bubble formation, and, most importantly, we are able to reach the size $N = 12000$ due to full symmetry exploitation. On the other hand, we set up the transfer matrix for three chains in a confined system with periodic boundary conditions on the surface of a cylinder with base circumference L. The largest eigenvalue of the transfer matrix (together with the corresponding eigenvector) yields the exact behaviour of the infinite chain system in the confined geometry. Extrapolations in the $L \to \infty$ limit are in general highly reliable within this approach [23–25] that allows to compute easily the free energy and the correlation length and to access the properties of the excited states as well (see Sect. 2). In particular, the transfer matrix approach within the confined system may allow to detect the geometrical scaling law for the energies of the Efimov triplet states, if present.

2 Methods

2.1 Directed Polymer Model

We model DNA chains within the Poland–Scheraga spirit [10] for directed self-avoiding polymers in a 1+1 square lattice. In particular, the strands move as shown in Fig. 1; at each step, their coordinates increase along the $(1, 1)$ direction (parallel direction in the following) so that the possible moves need to be along either $(1, 0)$ or $(0, 1)$. In this way, intra-chain self-intersections are forbidden and only inter-chain interactions between bases with the same monomer index are allowed, as it should happen for two complementary DNA strands.

Within our model, DNA strands can cross each other (see Fig. 1), get a Boltzmann weight $y = \exp(-\beta\epsilon)$ for each base pair interaction ($\epsilon < 0 \to y > 1$), and get a
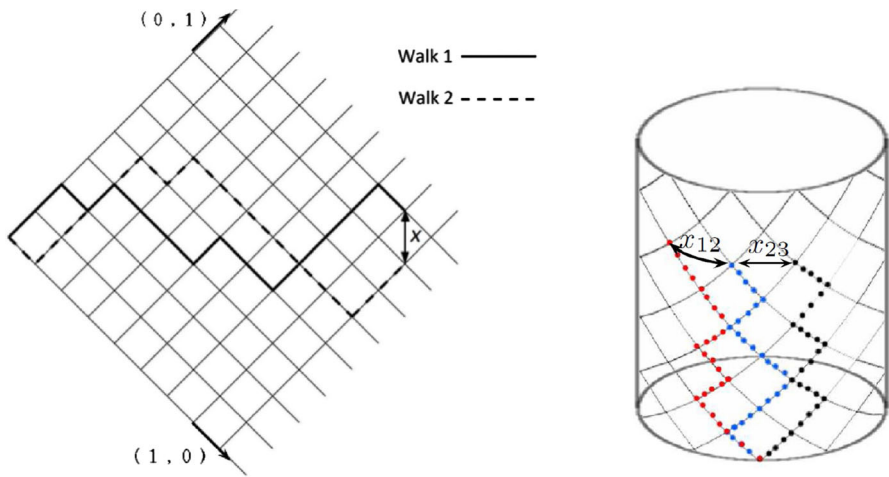
Fig. 1 DNA strands are self-avoiding walks (polymers) directed along the (1,1) direction of a two-dimensional square lattice. *Left* example for two DNA strands in unconfined geometry with end-to-end distance $x_{12} = x_2 - x_1 = -1$ along the transverse direction $(-1, 1)$. The Boltzmann weight of the shown conformation would be $y^4 \sigma^3$ if bubble opening is weighted or $y^4 \sigma^2$ if bubble closing is weighted. *Right* example for three DNA strands in the confined geometry with periodic boundary conditions resulting in a cylinder surface. The strands are directed along the cylinder axis while end-to-end distances $x_{12} = x_2 - x_1 = -1$, $x_{23} = x_3 - x_2 = -1$ are measured along the transverse direction. The Boltzmann weight of the shown conformation would be $y^6 w \sigma^5 \rho$ if bubble opening is weighted or $y^6 w \sigma^2$ if bubble closing is weighted (Colour figure online)

bubble fugacity σ whenever a bubble—a portion of single-stranded bases in between two double-stranded portions—is formed between strand pairs. We further introduce similar weights $w = \exp(-\beta \eta)$, for each base triplet interaction, and ρ, for three-chain bubble formation (a portion of either single- or double-stranded bases in between two triple-stranded portions). Bubble fugacity can be assigned alternatively to bubble opening (the strands split) or closing (the strands join), resulting in two different realizations of the model that, however, should yield exactly the same results in the thermodynamic limit.

The two-chain model in a $d+1$ directed euclidean lattice can be exactly solved in the thermodynamic limit of infinite chain length [16]. For such reason, similar models played an important role in clarifying melting, cold unzipping (opening induced by transverse force), and overstretching (induced by parallel force) properties of duplex DNA [26–30].

If bubble formation is not weighted ($\sigma = 1$), the two-chain model does not show any melting transition at finite temperatures in $1 + 1$ dimensions. In the quantum mechanics analogy, the dimension along which the polymers are directed plays the role of time: then it is well known that any short-range potential, no matter how weak, will produce a bound state for $d \leq 2$.

A bubble fugacity that disfavours bubble formation ($\sigma < 1$) and thus entropically destabilizes the double-stranded state is then needed to obtain a finite melting transition temperature (that is $y_{2,t} > 1$) in $d = 1$ for the two-chain system. The transition

temperature can be computed exactly in the thermodynamic limit:

$$y_{2,t} = \frac{2}{1+\sigma}. \tag{1}$$

In the following, we will use $\sigma = 1/2$, so that $y_{2,t} = 4/3$. We will always set $w = 1/y$, so that the energy of an interacting base triplet ($\approx -\ln\left(y^3\right) - \ln w \approx -2\ln y$) is *twice* the energy of an interacting base pair ($\approx -\ln y$). We will instead consider the two different cases:

$$\begin{aligned} \rho &= 1 & \Rightarrow & \quad \text{Model} \ \ A, \\ \rho &= 1/\sigma = 2 & \Rightarrow & \quad \text{Model} \ \ C. \end{aligned} \tag{2}$$

In our directed $1 + 1$ model, three-chain bubble formation involves the formation of two distinct two-chain bubbles as well, so that the corresponding overall weighting factor is $\sigma^2\rho$. As a result, three-chain bubbles are more penalized in Model A (σ^2 weight) than in Model C (σ weight).

In the absence of an exact solution for the three-chain model in the thermodynamic limit, one can follow two alternative strategies, both based on a transfer matrix approach, which can be easily set up in a directed polymer model:

– Evaluating exactly the partition function for three unconfined chains with N monomers each and extrapolate the results for $N \rightarrow \infty$. This involves the iteration of the transfer matrix N times. In the quantum analogy, it is equivalent to consider only finite time trajectories.
– Setting up the transfer matrix for a three-chain system *confined* within a lattice strip of width L along the transverse direction. The largest eigenvalue and the corresponding eigenvector of the transfer matrix yield the exact thermodynamic limit behaviour as $N \rightarrow \infty$. The thermodynamic limit for the unconfined system is then estimated by extrapolating the results for $L \rightarrow \infty$. This corresponds to consider full infinite time trajectories for quantum particles within a confined geometry.

Note that a single chain performs a random walk along the transverse direction so that one expects the general scaling $N \simeq L^2$ to hold when comparing the unconfined (N finite, $L = \infty$) and confined (L finite, $N = \infty$) systems.

2.2 Unconfined System

The canonical partition function can be written in general

$$Z_N = \sum_{x_{12}=-N}^{N} \sum_{x_{23}=-N}^{N} d_N(x_{12}, x_{23}), \tag{3}$$

where $x_{12} = x_2 - x_1$, $x_{23} = x_3 - x_2$ are the end-to-end distances (with sign) between chain pairs (1, 2), (2, 3), and the state vector $d_N(x_{12}, x_{23})$ is the partition function

for all configurations with fixed x_{12}, x_{23} (distances are measured along the transverse direction in units of the diagonal of the elementary square in the lattice, see Fig. 1).

For the unconfined system, the state vector $d_N (x_{12}, x_{23})$ can be obtained from the initial condition $d_0 (x_{12}, x_{23}) = y^3 w \delta_{x_{12},0} \delta_{x_{23},0}$ (the three chains start from the same point) through the iteration of the following recursion relation ($x_{13} = x_{23} + x_{12} = x_3 - x_1$):

$$
\begin{aligned}
d_N(x_{12}, x_{23}) = \big[& 2d_{N-1}(x_{12}, x_{23}) + d_{N-1}(x_{12} - 1, x_{23}) \sigma^{\delta_{x_{12},1} + \delta_{x_{13},1}} \rho^{\delta_{x_{12},1} \delta_{x_{13},1}} \\
& + d_{N-1}(x_{12} + 1, x_{23}) \sigma^{\delta_{x_{12},-1} + \delta_{x_{13},-1}} \rho^{\delta_{x_{12},-1} \delta_{x_{13},-1}} \\
& + d_{N-1}(x_{12}, x_{23} - 1) \sigma^{\delta_{x_{23},1} + \delta_{x_{13},1}} \rho^{\delta_{x_{23},1} \delta_{x_{13},1}} \\
& + d_{N-1}(x_{12}, x_{23} + 1) \sigma^{\delta_{x_{23},-1} + \delta_{x_{13},-1}} \rho^{\delta_{x_{23},-1} \delta_{x_{13},-1}} \\
& + d_{N-1}(x_{12} + 1, x_{23} - 1) \sigma^{\delta_{x_{12},-1} + \delta_{x_{23},1}} \rho^{\delta_{x_{12},-1} \delta_{x_{23},1}} \\
& + d_{N-1}(x_{12} - 1, x_{23} + 1) \sigma^{\delta_{x_{12},1} + \delta_{x_{23},-1}} \rho^{\delta_{x_{12},1} \delta_{x_{23},-1}} \big] \\
& \times y^{\delta_{x_{12},0} + \delta_{x_{23},0} + \delta_{x_{23},0}} w^{\delta_{x_{12},0} \delta_{x_{23},0}} .
\end{aligned}
\tag{4}
$$

The above equation employs bubble opening to weigh bubble formation. A similar equation can be written if bubble closing is employed. For a given N, we will compute the average squared end-to-end distance:

$$
r_N^2 = \frac{\sum_{x_{12}=-N}^{N} \sum_{x_{23}=-N}^{N} \frac{x_{12}^2 + x_{23}^2 + x_{13}^2}{3} d_N(x_{12}, x_{23})}{\sum_{x_{12}=-N}^{N} \sum_{x_{23}=-N}^{N} d_N(x_{12}, x_{23})} .
\tag{5}
$$

In practice, one can exploit the symmetries of the system (exchange symmetry of the three chains and the mirror symmetry by changing transverse coordinate signs) to define state vectors with reduced dimensions and considerably speed up their computation. The recursion equations need to be changed accordingly, similarly to what is described in detail below for the confined system. For the unconfined system, we managed to compute the state vectors and the average squared end-to-end distance up to $N = 12000$.

2.3 Transfer Matrix for the Confined System

In the confined system we use periodic boundary conditions along the transverse direction, so that the chains move along the surface of a cylinder with base circumference L (see Fig. 2). We consider all possible symmetries of the system (exchange symmetry of the three chains, mirror symmetry due to the change of distance sign, $x \to -x$, and to the periodic boundary, $x \to L - x$) to restrain the possible states within the triangle in the (r_m, r_s) plane shown in Fig. 2, with vertexes in $(0, 0)$, $(L/3, L/3)$ and $(L/2, 0)$ and edges given by $r_s = 0$, $r_s = r_m$, $r_s = L - 2r_m$. Upon using symmetries, r_s, r_m are the smallest, medium (respectively) distances between chain pairs. The whole discussion below relies on choosing L as a multiple of 6.

The recursion relation for $d_N (r_m, r_s)$ needs to take into account how many different configurations are possible, related to each other by symmetries, in the full (x_{12}, x_{23}) state plane, for a given choice of (r_m, r_s).
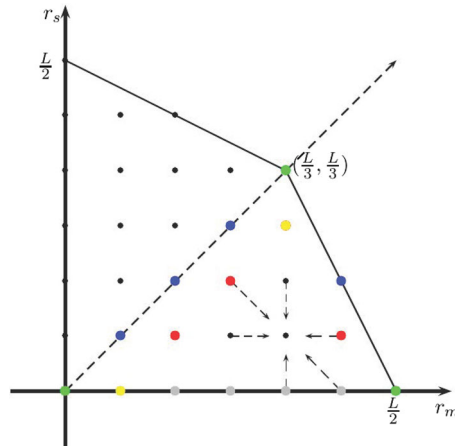
Fig. 2 Allowed states in the (r_m, r_s) plane can be restricted by using symmetry considerations to points within the triangle with coloured sides. *Different colours* represent different properties with respect to symmetry and consequently different factors to be used in Eq. (8) according to Eqs. (6,7). *Dashed arrows* represent all possible (r_m, r_s) states from which a given (r'_m, r'_s) state can be reached. *Each arrow* describes a different summand weighted by the corresponding $b(r_m, r_s, r'_m, r'_s)$ factor in Eq. (8) (Colour figure online)

Different colours in Fig. 2 show states which have special symmetry properties in the recursion relation. In order to write the latter, it is useful to define the functions $f(r_m, r_s)$ that takes into account how symmetry affects the staying in the same state, and $b(r_m, r_s, r'_m, r'_s)$ that takes into account how symmetry affects the going from state (r_m, r_s) to state (r'_m, r'_s) (see Fig. 2):

$$
f(r_m, r_s) = \begin{cases}
3 & \text{if } (r_m, r_s) \in \text{red dots} \\
4 & \text{if } (r_m, r_s) = (L/3, L/3 - 1) \text{ upper yellow dot} \\
2 + 2\sigma & \text{if } (r_m, r_s) = (1, 0) \text{ lower yellow dot} \\
2 & \text{otherwise}
\end{cases}
\tag{6}
$$

$$
b(r_m, r_s, r'_m, r'_s) = \begin{cases}
2 & \text{if } (r_m, r_s) \in \text{edge} \wedge (r'_m, r'_s) \notin \text{same edge} \\
6 & \text{if } (r_m, r_s) = (0, 0) \,||\, (r_m, r_s) = (L/3, L/3): \\
  & \qquad\qquad\qquad\quad \text{from green to yellow} \\
2 & \text{if } (r_m, r_s) = (L/2, 0) \wedge (r'_m, r'_s) = (r_m - 1, r_s): \\
  & \qquad\qquad\qquad\quad \text{from green to grey} \\
4 & \text{if } (r_m, r_s) = (L/2, 0) \wedge (r'_m, r'_s) = (r_m - 1, r_s + 1): \\
  & \qquad\qquad\qquad\quad \text{from green to red} \\
0 & \text{if } (r_m, r_s) \text{ outside the triangle} \\
1 & \text{otherwise}
\end{cases}
\tag{7}
$$

Then the recursion equation for $d_N(r_m, r_s)$ can be written as (note that $r_m = 0 \Rightarrow r_s = 0$):

$$
\begin{aligned}
d_N\left(r_m, r_s\right) = \big[& f\left(r_m, r_s\right) d_{N-1}\left(r_m, r_s\right) \\
& + d_{N-1}\left(r_m, r_s-1\right) \sigma^{\delta_{r_s,1}} b\left(r_m, r_s-1, r_m, r_s\right) \\
& + d_{N-1}\left(r_m-1, r_s\right) \sigma^{2\delta_{r_m,1}} \rho^{\delta_{r_m,1}} b\left(r_m-1, r_s, r_m, r_s\right) \\
& + d_{N-1}\left(r_m+1, r_s-1\right) \sigma^{\delta_{r_s,1}} b\left(r_m+1, r_s-1, r_m, r_s\right) \\
& + d_{N-1}\left(r_m, r_s+1\right) b\left(r_m, r_s+1, r_m, r_s\right) \\
& + d_{N-1}\left(r_m+1, r_s\right) b\left(r_m+1, r_s, r_m, r_s\right) \\
& + d_{N-1}\left(r_m-1, r_s+1\right) b\left(r_m-1, r_s+1, r_m, r_s\right) \big] \\
& \times y^{\delta_{r_s,0}+2\delta_{r_m,0}} w^{\delta_{r_m,0}} .
\end{aligned} \tag{8}
$$

The above equation employs bubble opening to weigh bubble formation. A similar equation can be written if bubble closing is used instead. We can now define the transfer matrix for the three-chain system, so that

$$
\begin{aligned}
d_N\left(r_m', r_s'\right) &= \sum_{r_m, r_s} T_{r_m' r_s', r_m r_s} d_{N-1}\left(r_m, r_s\right) \\
d_N(a) \quad &= \sum_b T_{ab} d_{N-1}(b) = \sum_b T_{ab}^N d_0(b) ;
\end{aligned} \tag{9}
$$

where the indexes a, b run over all states of the symmetrized system.

The total number of states M is equal to the number of points inside the triangular domain of area A:

$$
M = A + L/2 + 1 = (L^2/12) + L/2 + 1 . \tag{10}
$$

For $L = 1980$, the largest size used in this work, $M = 327691$.

The transfer matrix T is non-negative, real and not symmetric. It can be shown, however, that T can be symmetrized [31]. As a result, the eigenvalues and eigenvectors of T are real, as we indeed find. Interestingly, the change in bubble weighting (either opening or closing) does not affect the computed eigenvalues and eigenvectors, and the symmetrized matrix is the same in both cases. This is indeed expected, since in the $N \to \infty$ limit the two model realizations have to yield the same results, even for finite L.

We are interested in computing the eigenvalues $\lambda_{i,L}$ and the corresponding right eigenvectors $v_{i,L}(a)$. Eigenvalues are ranked so that $i = 1$ corresponds to the largest, $i = 2$ to the second largest, and so on. The largest eigenvalue is related to the ground state, and all the components of the corresponding eigenvector are positive [31].

In the thermodynamic limit of infinite chain length $N \to \infty$, one can exactly compute the free energy at fixed L as the ground state free energy $f_{1,L} = -\ln \lambda_{1,L}$, the correlation length $\xi_{\parallel,L} = 1/\ln\left(\lambda_{1,L}/\lambda_{2,L}\right)$ along the parallel direction, the average squared smallest distance $r_{s,L}^2 = \frac{\sum_a r_s^2(a) v_{1,L}(a)}{\sum_a v_{1,L}(a)}$ between chain pairs.

A generic eigenvector i is a bound state if its free energy $f_{i,\infty} = -\ln \lambda_{i,\infty}$ is lower than the free energy $-3\ln 2$ of 3 non-interacting chains in the limit of infinite strip width that is if $\ln\left(8/\lambda_{i,\infty}\right) < 0$.

Note that due to the scaling relation $N \simeq L^2$, one expects quantities such as $\xi_{\parallel,L}$, $r_{s,L}^2$ to scale with L^2 in the limit of infinite strip width.

3 Results

3.1 Model A Does not Have Efimov-Like Behaviour

For Model A, we computed the average squared end-to-end-distance r_N^2 for three unconfined chains up to a chain length $N = 12000$, using two different ways to weigh bubble formation. Finite size estimates of the three-chain transition temperature $y_{3,t}$ were obtained by looking at the crossing of the curves $r_N^2(y)/N$ for different sizes, as already done [5]:

$$\frac{r_N^2(y_{3,t})}{N} = \frac{r_{N-1}^2(y_{3,t})}{N-1} .$$ (11)

The results are reported in the top panel of Fig. 3 as a function of $1/N$. Finite size estimates of $y_{3,t}$ depend on how bubble formation is weighted, as expected. Both curves exhibit an unusual non-monotonic "backbending" such that y_3, t is initially decreasing for small N and then increasing for larger N, after having reached a minimum (barely visible on the shown scale for the black curve). This feature makes extrapolations in the infinite size limit a delicate issue. In particular, if finite size estimates are available only for sizes smaller than the "backbending size", the resulting extrapolation may end up being grossly wrong. If, for example, the red curve is extrapolated based only on $N < 4000$ (that is $1/N > 0.00025$), one gets an apparently clear indication that $y_{3,t} < 4/3$ with an estimate of the difference roughly consistent with the one, $(-7 \pm 1) \cdot 10^{-4}$, reported in [5]. Yet, the availability of the data for $N \leq 12000$, with the consequent uncovering of the "backbending" feature, allows to clearly rule out that estimate. A quantitative assessment of whether $y_{3,t} < 4/3$ or not for Model A in the infinite size limit is still made difficult by the non-monotonic behaviour, so that polynomial extrapolations (not shown) strongly depend on the range of the sizes used for the fit and on polynomial order.

We thus considered, again for Model A, the system of three chains of infinite length confined on a cylinder surface of base circumference L. We obtained finite size estimates of $y_{3,t}$ in a similar way, by computing the average squared smallest end-to-end distance $r_{s,L}^2$ among the three possible chain pairs and looking at the crossing of the curves $r_{s,L}^2(y)/L^2$ for different sizes:

$$\frac{r_{s,L}^2(y_{3,t})}{L^2} = \frac{r_{s,L-6}^2(y_{3,t})}{(L-6)^2} .$$ (12)

L needs to be a multiple of 6 in order to properly exploit symmetries. L^2 needs to be used at the denominator because the typical length explored by a chain of length N along the transverse direction is $\approx N^{1/2}$ in the high temperature random walk regime, so that a finite chain length N in the unconfined system should roughly correspond to a finite size $L \approx N^{1/2}$ for the confined case.
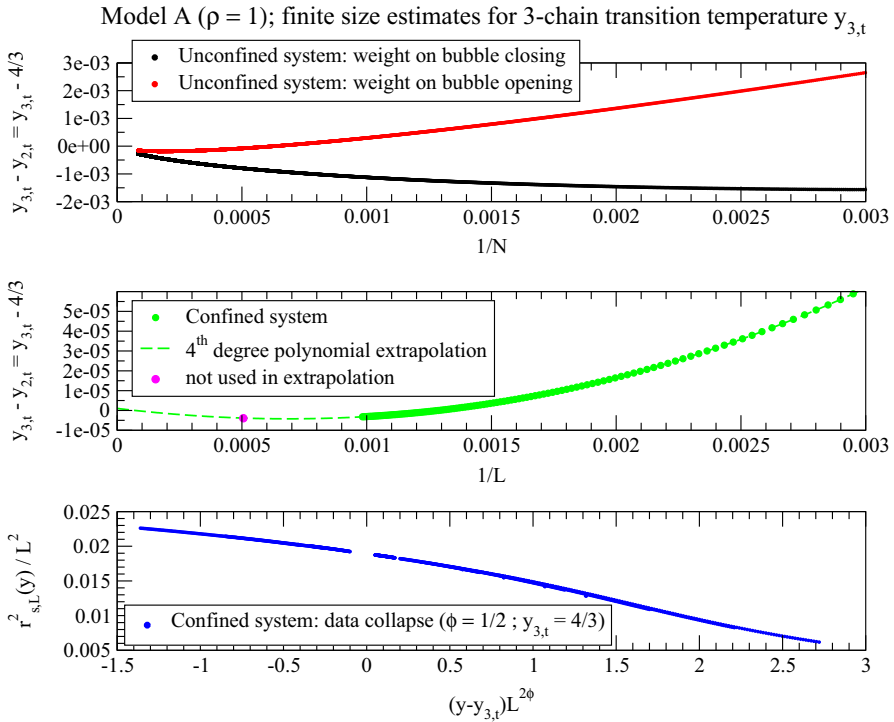
Fig. 3 In model A, the transition temperature $y_{3,t}$ of the three-chain system is the same as in the two-chain system $y_{2,t} = 4/3$ ($y_{3,t} - y_{2,t}$ is reported). *Top panel* finite size estimates of transition temperature for three chains in the unconfined system obtained by using the crossing of $< r_N^2 > /N$ and $< r_{N+1}^2 > /(N+1)$ curves; both possibilities for bubble weighting are shown: weight on bubble closing (*black*) and on bubble opening (*red*). *Middle panel* finite size estimates of transition temperature for three chains in the confined system obtained by using the crossing of $< r_{s,L}^2 > /L^2$ and $< r_{s,L-6}^2 > /(L-6)^2$ curves; the *green points* ($330 \leq L \leq 1020$) are used to obtain the 4th-degree polynomial extrapolation (*dashed line*): the magenta point is obtained for $L = 1980$ to test the polynomial extrapolation. *Bottom panel* data collapse of the $< r_{s,L}^2 > /L^2$ curves for three chains in the confined system as a function of y; 123 different L and nine different y values are used (Colour figure online)

The results are reported in the middle panel of Fig. 3 as a function of $1/L$. Note that finite size estimates for the confined system do not depend on how bubble formation is weighted, because the infinite chain limit has been already taken when considering the largest eigenvalue of the transfer matrix. A non-monotonic "backbending" is hinted at by the reported data for $L \leq 1020$ (green points), similarly to the unconfined case. However, the difference $y_{3,t} - 4/3$ that can be assessed in the confined case is lower by a 100 factor, roughly. In fact, a reliable polynomial extrapolation (dashed line) of the non-monotonic behaviour can be obtained by fitting the data for sizes *smaller* than the backbending size. Extrapolation reliability is tested through the excellent comparison with the actual estimate, *not* used in the extrapolation, computed for a size ($L = 1980$, magenta circle), *larger* than the backbending size. The reported extrapolation allows us to conclude that $y_{t,3} = 4/3$ within an accuracy of $2 \cdot 10^{-6}$.

A further evidence that Efimov-like behaviour is not present in Model *A* for directed chains on a 1 + 1 square lattice and that the three-chain melting transition share the same properties as the two-chain one is obtained through data collapse. As shown in the bottom panel of Fig. 3, all data for $r_{s,L}^2(y)$ in the confined system that were used to obtain finite size estimates of $y_{3,t}$ collapse almost perfectly on a single scaling function $g(t)$ according to the scaling law

$$\frac{r_{s,L}^2(y)}{L^2} = g\left((y - y_{3,t})L^{2\phi}\right) , \tag{13}$$

where ϕ is the crossover exponent [16].

The collapse shown in Fig. 3 is obtained using $y_{3,t} = 4/3$ and $\phi = 1/2$, as it would be the case for the two-chain melting transition [16] and involve 123 different sizes for 9 different y values. By optimizing the quality of the data collapse [32] with respect to both ϕ and $y_{3,t}$ for $L \leq 1020$ data, we obtain the estimates $y_{3,t} = 1.33333302$, $2\phi = 1.03854$. Taken together, the evidence we reported for Model *A* showing a three-chain melting transition at the same temperature as the two-chain one is fairly convincing.

3.2 Model *C* has Efimov-Like Behaviour

We then studied Model *C* in the confined case. We obtained finite size estimates of $y_{3,t}$ in a different way, by computing the correlation length $\xi_{\parallel,L}$ in the parallel direction for a finite size L, and looking at the crossing of the curves $\xi_{\parallel,L}(y)/L^2$ for different sizes:

$$\frac{\xi_{\parallel,L}(y_{3,t})}{L^2} = \frac{\xi_{\parallel,L-6}(y_{3,t})}{(L-6)^2} . \tag{14}$$

The $y_{3,t}$ estimate obtained by crossing the end-to-end distance curves yielded very accurate results for Model *A*, but it requires the computation of the ground state eigenvector for several y values at each different size. The computation of the correlation length $\xi_{\parallel,L}$ requires the two largest eigenvalues of the transfer matrix and is thus computationally cheaper. Estimating critical parameters by the crossing of correlation length curves at different sizes is a well-known phenomenological renormalization procedure [24,25].

The finite size estimates of $y_{3,t}$ obtained in this way in the confined case are reported in the top panel of Fig. 4 for both Model *A* (black) and Model *C* (red). Backbending is actually present in this case as well for Model *A*, but the backbending size is very small and left out of the scale of the plot. Backbending is instead not present for Model *C*. Polynomial extrapolations, based on $84 \leq L \leq 378$, are shown as dashed lines. In the infinite size limit $L \to \infty$, we recover the result that $y_{3,t} = 4/3$ for Model *A*, even though with less accuracy ($2 \cdot 10^{-5}$) than for the end-to-end distance data. Model *C* data clearly demonstrate a higher transition temperature, resulting in the infinite size estimate $y_{3,t} - 4/3 = (-4.8 \pm 0.2) \cdot 10^{-4}$. Since systematic errors are necessarily involved in extrapolating finite size data, we associate to the latter estimate the same accuracy with which Model *A* estimate allows to confirm that $y_{3,t} = 4/3$.
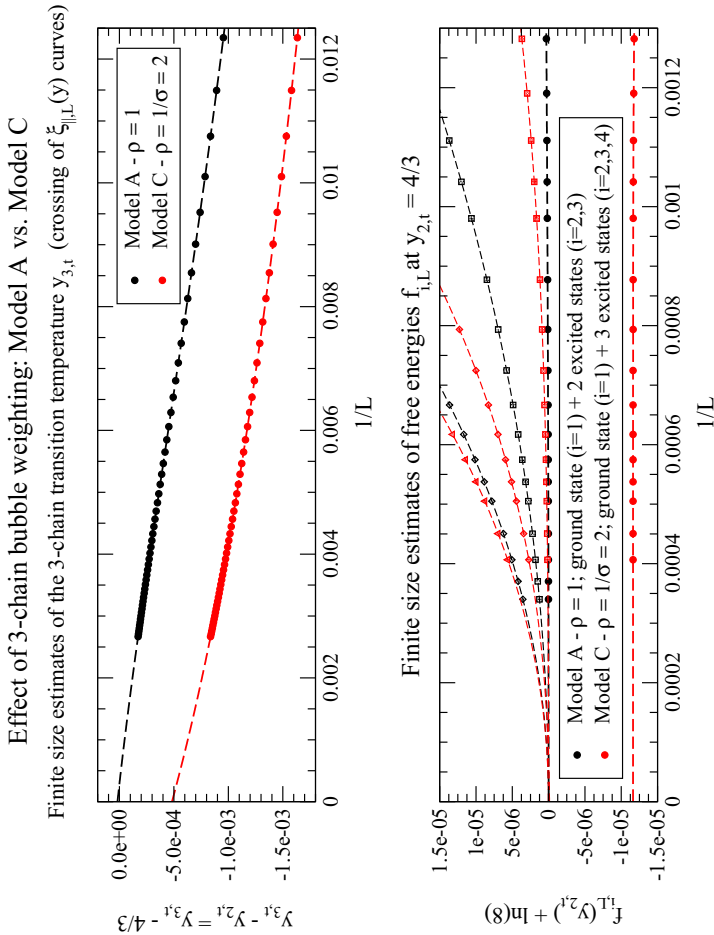
Fig. 4 Different behaviour between Model A (*black*) and Model C (*red*) as evidenced in the confined system. *Top panel* finite size estimates of the difference $y_{3,t} - y_{2,t}$ between $y_{3,t}$, the three-chain transition temperature and $y_{2,t} = 4/3$, the two-chain one, obtained by using the crossing of $< \xi_{\parallel,L}^2 > / L^2$ and $< \xi_{\parallel,L-6}^2 > / (L-6)^2$ curves; polynomial 4-th degree extrapolations obtained for $84 \leq L \leq 378$ are shown (*dashed lines*). *Bottom panel* free energies $f_{i,L}$ evaluated at the critical transition point $y_{2,t} = 4/3$ of the two-chain system for both the ground state ($i = 1$) and the first excited states ($i = 2, 3$ for Model A and $i = 2, 3, 4$ for Model C); $f_{i,L} + \ln 8 < 0$ for a bound state: non-linear extrapolation—see main text—obtained for $780 \leq L \leq 2460$ is shown for Model C ground state (*dashed line*); polynomial 6-degree extrapolations are shown for all other states (*dashed lines*) (Colour figure online)

The different behaviour of Model A and Model C is confirmed from another perspective in the bottom panel of Fig. 4, where we plot the finite size estimates of the free energies of the ground states and the first excited states for both models at the two-chain critical temperature $y_{2,t} = 4/3$. More precisely, we plot the free energy difference with respect to the three-chain unbound state, whose free energy is $-3 \ln 2 = -\ln 8$, being determined by the entropy of 3 isolated strands:

$$f_{i,L}(y_{2,t}) + \ln 8 = \ln\left(\frac{8}{\lambda_{i,L}(y_{2,t})}\right), \tag{15}$$

where $\lambda_{i,L}$ is the i-th largest eigenvalue of the transfer matrix. Negative values in the infinite size limit signal the presence of a bound state, whereas extrapolation to zero difference is expected for unbound states.

The data clearly show that the ground state of model C is a bound state at $y = 4/3$, consistent with the Efimov-like picture. An extrapolation of finite size data using $f_{1,L} = A_0 - A_1 \exp(-L/A_2)$ (dashed line) yields $f_{i,L}(y_{2,t}) + \ln 8 = A_0 = (-1.163 \pm 0.001) \times 10^{-5}$. On the other hand, the ground state of model A can be shown to be unbound, that is $f_{1,L} + \ln 8 = 0$ within an accuracy of 2×10^{-10} upon polynomial extrapolation, again consistently with the absence of Efimov-like behaviour. All excited states display the features of unbound states for both models, that is $f_{1,L} + \ln 8 = 0$ upon polynomial extrapolation within an accuracy varying from 1×10^{-7} to 2×10^{-9}, with a remarkable one-to-one correspondence in the spectrum of unbound states between the two models.

The different melting transition properties of Model A and C can be easily visualized at a glance by looking at probability distributions, as given by ground state eigenvectors. We report them in Fig. 5 for $L = 420$. System microstates are defined in the $(r_{\mathrm{m}}, r_{\mathrm{s}})$ plane through the smallest, r_{s}, and middle, r_{m}, end-to-end distances among the three pairs of chains. The minimal set of microstates that can be used to describe the whole system by means of symmetry properties is defined within the triangle shown in Fig. 2 (see Sect. 2). The triplet interaction microstate corresponds to the lower left triangle vertex. The microstates on the lower triangle edge represent a base pair interaction with the third strand on its own. In the microstate represented by the top triangle vertex, all strand pairs are equally far apart.

In the high temperature regime ($y = 1.33 < y_{3,t}$ for both models), the eigenvector components describe a delocalized macrostate, corresponding to three single-stranded chains, that is very similar within both models: the most probable microstate is the top triangle vertex.

At the transition point of the two-chain system ($y = y_{2,t} = 4/3$), however, the two models behave quite differently, as already signalled by the largest eigenvalue behaviour. This is the melting transition point for Model A as well, and the ground state eigenvector is indeed characterized by an almost evenly distributed probability across all microstates. At the melting transition of the two-chain system one would indeed get an exactly uniform probability distribution across all possible end-to-end
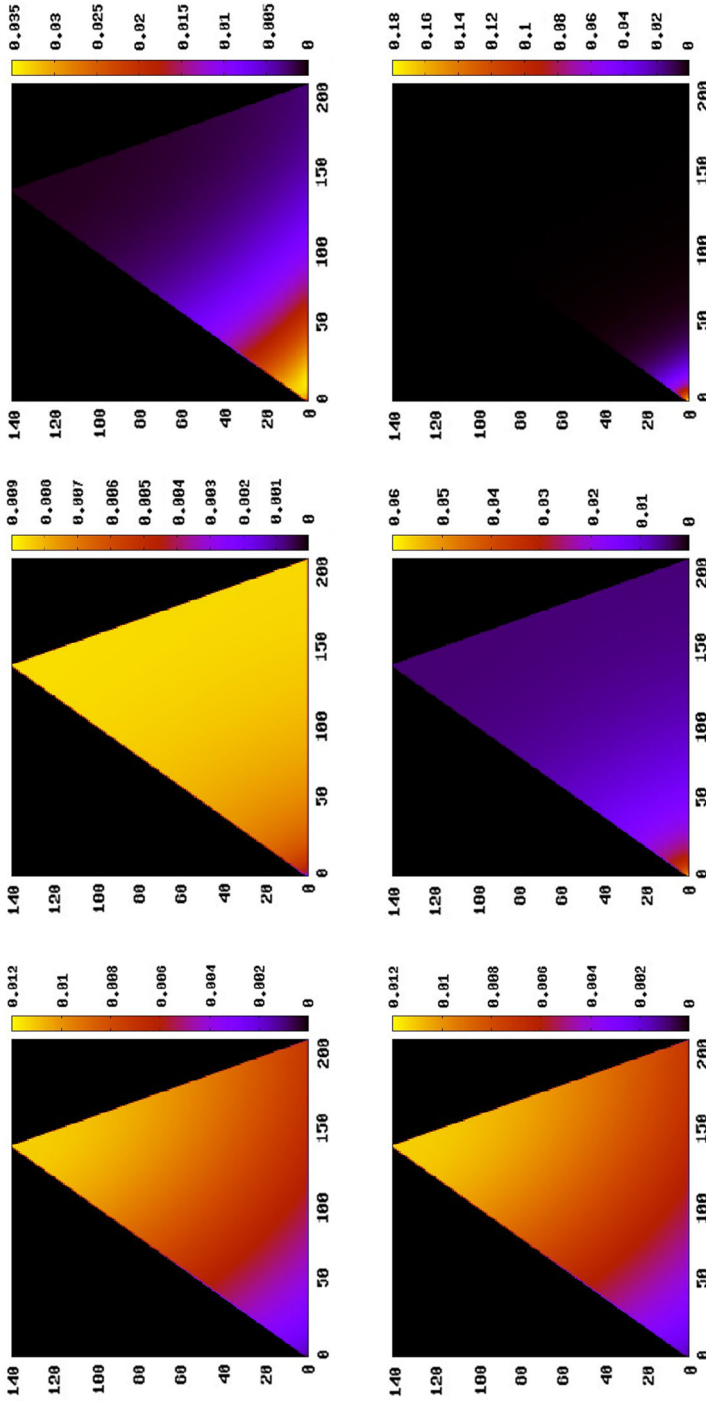
Fig. 5 Ground state eigenvector components for the confined three-chain system at $L = 420$. Different microstates of the system are represented within the same *triangle* already described in Fig. 2, in the plane (r_m, r_s) (see Sect. 2). The microstate of base triplet interaction is represented by the *bottom left triangle* vertex. The brighter the colour, the higher the eigenvector component. The colour scale may vary in different plots. *Top row* Model A. *Bottom row* Model C. *Left column* $y = 1.33$ (high temperature unbound state in both models). *Middle column* $y = y_2$, $t = 4/3$ (transition temperature for Model A, triplet bound state for Model C). *Right column* $y = 1.34$ (triplet bound state for both models) (Colour figure online)

distance values.[3] For Model C, instead, $4/3 > y_{3,t}$ and the corresponding ground state indeed clearly describes a triplet bound state whose probability is localized in the lower left triangle corner and rapidly decays away from it.

In the low temperature regime, $y = 1.34 > y_{3,t}$ for both models and a triplet bound state is clearly seen accordingly. However, the localization extent of the ground state is much higher for model C, evidencing again that the triplet bound state is more stable than in model A.

4 Discussion

We studied two different models for three directed polymer chains in the $1 + 1$ square lattice. Directedness allows inter-chain interactions only between monomers with the same index along the chain, thus mimicking base pair interaction between complementary DNA strands. For the same reason, it is possible to map the DNA-like polymer problem to a quantum problem of interacting particles where monomer index is imaginary time and chain configurations are particle trajectories. Thermal fluctuations in the polymer problem are akin to quantum fluctuations.

The two studied models differ only in three-chain bubble formation being more penalized in Model A with respect to Model C. Weighting bubble opening or closing is necessary in low dimension, in order to have a finite transition temperature (in the quantum analogy any attractive potential no matter how weak would admit a bound ground state). In principle, the analogue of bubble weighting could be introduced in the quantum problem as well (see Footnote 1).

We extended previous transfer matrix computations for Model A for a finite unconfined system to bigger chain lengths, by fully exploiting all symmetries. Moreover, we implemented the transfer matrix technique for a confined system with periodic boundary conditions. This allowed us to compute exact results in the thermodynamic limit for the confined system. Full considerations of system symmetries allowed to reach system sizes that are effectively much larger than in the unconfined case. In addition, free energies and probability distributions were easily obtained through the largest eigenvalue and the corresponding eigenvector of the transfer matrix.

Thanks to the combination of both approaches, we showed that the minute piece of evidence shown in [5] for the presence of Efimov-like behaviour in Model A was an artefact based on not having reached too large chain lengths and on a subtle back-bending effect in the thermodynamic limit convergence of the transition temperature estimates for finite systems. Model A does not show any Efimov-like behaviour on the Sierpinski gasket as well [8].

We further showed that Model C displays Efimov-like behaviour, again in agreement with what we had found on the Sierpinski gasket. Moreover, the transfer matrix approach in the confined system allowed us to show that only one triple-stranded DNA

---

[3] At the melting transition, the two-chain problem is equivalently described by a fully unbiased ($y = 1$, $\sigma = 1$) random walk, thus yielding a uniform probability distribution at equilibrium in a finite size system with periodic boundary conditions

state is stable, just above the double-stranded melting temperature. We are thus not recovering the full quantum Efimov picture, indeed not expected to hold in $d = 1$.

Our results show that the three-body polymer physics is subtle. The temperature window and the energy difference involved in the effect that we uncover are very narrow. Our results further underline how the details of bubble weighting are crucial in driving the Efimov-like behaviour in low d and how the nature of the lattice is not a relevant factor, at least for $d \leq 1$ ($d + 1 = \ln 3/ \ln 2$ in the Sierpinski). They also lead to the further questions of what is the origin of the Efimov-like feature that we are observing and whether and upon which conditions the full Efimov picture could be observed in polymer physics. Relevant factors are most likely dimension and particle statistics, besides bubble weighting.

In this respect, we observe that the transfer matrix for confined system that we set up in this work is a promising approach, capable of reaching a very good accuracy in the extrapolation to the infinite size limit, within a reasonable computational effort. Combined with proper symmetry considerations, it may be a valuable strategy to investigate the possible emergence of the full Efimov physics in polymer models for both the standard problem for identical particles in higher dimension and a suitably modified Calogero problem for non-identical particles in $d = 1$, where the full Efimov picture holds [33]. On the other hand, confined geometries "per se" are an interesting playground for further studies of the quantum Efimov physics [34], making the corresponding investigation of the polymer Efimov analogy straightforward within the transfer matrix approach.

In a broader perspective, one may ask whether the melting of an actual triple-stranded DNA molecule could indeed take place at a temperature higher than for the corresponding double-stranded one. Further work is needed to properly assess such speculation, especially given the sensitivity of the shown results to model details.

Distinctive features of real DNA molecules that are not considered in the simplified models presented here are sequence heterogeneity and the semiflexibility of double-stranded DNA resulting in its persistence length being around 50 nm, or 150 base pairs (triple-stranded DNA should behave similarly in this respect).

In principle, a bending rigidity term can be easily included in the present transfer matrix approach, whereas sequence heterogeneity could be included only for unconfined systems, when the matrix is explicitly used at each step. Qualitatively, however, we do not expect any of the above features to alter the basic nature of a bubble driven transition that is at the basis of the polymer Efimov effect.

As long as bubble size gets much bigger than the persistence length, double-stranded DNA rigidity becomes irrelevant. Moreover, the single-stranded DNA portions that make up a bubble are essentially flexibles, with a persistence length of around 2 nm, or $4 - 5$ bases.

The melting transition of a double-stranded heterogeneous DNA was studied by introducing random interactions [35]. Although there are subtle changes (disorder is a "marginally relevant variable" in $d = 1$), the basic feature of a bubble driven transition is again preserved. This is because the heterogeneity involves merely a distribution of the strength of base pair attraction and there is no other competition.

One essential ingredient in our approach is strict DNA strand complementarity, at the basis of the quantum analogy. In this respect, we observe that in modelling realistic

DNA molecules, one should think of one monomer in our model as the coarse-grained representation of a stretch of several DNA bases. In this way, the lack of interaction between monomers with different chain indexes and the absence of the helical structure (or at least of some reduction in chain flexibility) in the double- and triple-stranded phases can be more easily rationalized.

An equally important and delicate issue concerns a realistic estimate of model parameters. The value of the two-chain cooperativity parameter σ is typically very low ($\simeq 10^{-5}$) in realistic applications [17], thereby suggesting that bubble formation is highly suppressed. On the other hand, a proper estimate of the three-chain cooperativity parameter ρ would require a careful analysis of the experimental melting curves for triplex DNA, together with the knowledge of the thermodynamics parameters associated to both Watson–Crick and Hoogsteen pairings. The latter are considered equivalent in the results shown here.

Finally, temperature is not the only actor playing a role in stabilizing double- and triple-stranded DNA helices. Inter- and intra-helices interactions are sensitive to the presence of cations that may trigger the precipitation of DNA helices into a condensed phase [36]. In particular, divalent cations are not able to condense double-stranded DNA, whereas they succeed in doing so with triple-stranded DNA [37]. This points again to a higher stability of the latter, at least in the condensed phase stabilized by counterion mediated inter-helical attractions.

References

1. V. Efimov, Phys. Lett. B **33**, 563 (1970)
2. E. Braaten, H.-W. Hammer, Ann. Phys. **322**, 120 (2007)
3. D.V. Fedorov, A.S. Jensen, K. Riisager, Phys. Rev. Lett. **73**, 2817 (1994)
4. T. Kraemer, M. Mark, P. Waldburger, J.G. Danzl, C. Chin, B. Enseger, A.-D. Lange, K. Pilch, A. Jaakkola, H.-C. Nägerl, R. Grimm, Nature **440**, 315 (2006)
5. J. Maji, S.M. Bhattacharjee, F. Seno, A. Trovato, New J. Phys. **12**, 083057 (2010)
6. J. Maji, S.M. Bhattacharjee, Phys. Rev. E **86**, 041147 (2012)
7. T. Pal, P. Sadhukhan, S.M. Bhattacharjee, Phys. Rev. Lett. **110**, 028105 (2013)
8. J. Maji, S.M. Bhattacharjee, F. Seno, A. Trovato, Phys. Rev. E **89**, 012121 (2014)
9. T. Pal, P. Sadhukhan, S.M. Bhattacharjee, Phys. Rev. E **91**, 042105 (2015)
10. D. Poland, H.A. Scheraga, J. Chem. Phys. **85**, 1456 (1966)
11. M.D. Frank-Kamenetskii, S.M. Mirkin, Annu. Rev. Biochem. **64**, 65 (1995)
12. I. Radhakrishnan, D.J. Patel, Biochemistry **33**, 11405 (1994)
13. E.N. Nikolova, F.L. Gottardo, H.M. Al-Hashimi, J. Am. Chem. Soc. **134**, 3667 (2012)
14. D.P. Arya, R.L. Coffee, L. Xue, Bioorg. Med. Chem. Lett. **14**, 4643 (2004)
15. A. Jain, G. Wang, K.M. Vasquez, Biochimie **90**, 1117 (2008)
16. D. Marenduzzo, A. Trovato, A. Maritan, Phys. Rev. E **64**, 031901 (2001)
17. R.D. Blake, J.W. Bizzaro, J.D. Blake, G.R. Day, S.G. Delcourt, J. Knowles, K.A. Marx, J. SantaLucia Jr., Bioinformatics **15**, 370 (1999)
18. E. Braaten, H.-W. Hammer, Phys. Rep. **428**, 259 (2006)
19. Y. Kafri, D. Mukamel, L. Peliti, Eur. Phys. J. B **27**, 135 (2002)
20. A. Hanke, M.G. Ochoa, R. Metzler, Phys. Rev. Lett. **100**, 018106 (2008)
21. M.E. Fischer, J. Stat. Phys. **34**, 667 (1984)
22. S. Mukherji, S.M. Bhattacharjee, Phys. Rev. E **48**, 3427 (1993)

23. B. Derrida, J. Phys. A **14**, L5 (1981)
24. A. Trovato, F. Seno, Phys. Rev. E **56**, 131 (1997)
25. C. Vanderzande, *Lattice Models of Polymers* (Cambridge University Press, Cambridge, 1998)
26. S.M. Bhattacharjee, J. Phys. A **33**, L423 (2000)
27. D. Marenduzzo, S.M. Bhattacharjee, A. Maritan, E. Orlandini, F. Seno, Phys. Rev. Lett. **88**, 028102 (2001)
28. R. Kapri, S.M. Bhattacharjee, F. Seno, Phys. Rev. Lett. **93**, 248102 (2004)
29. D. Marenduzzo, A. Maritan, E. Orlandini, F. Seno, A. Trovato, J. Stat. Mech. **2009**, L04001 (2009)
30. D. Marenduzzo, E. Orlandini, F. Seno, A. Trovato, Phys. Rev. E **81**, 051926 (2010)
31. R.A. Horn, C.A. Johnson, *Matrix Analysis* (Cambridge University Press, Cambridge, 2013)
32. S.M. Bhattacharjee, F. Seno, J. Phys. A **34**, 6375 (2001)
33. S. Moroz, J.P. D'Incao, D.S. Petrov, Phys. Rev. Lett. **115**, 180406 (2015)
34. J. Levinsen, P. Massignan, M.M. Parish, Phys. Rev. X **4**, 031020 (2014)
35. S.M. Bhattacharjee, S. Mukherji, Phys. Rev. Lett. **70**, 49 (1993)
36. A.G. Cherstvy, A.A. Kornyschev, S. Leikin, J. Phys. Chem. B **106**, 13362 (2002)
37. X. Qiu, V.A. Parsegian, D.C. Rau, Proc. Natl. Acad. Sci. USA **107**, 21482 (2010)